Nanoscale Advances

ROYAL SOCIETY OF CHEMISTRY

PAPER

View Article Online
View Journal | View Issue

Cite this: *Nanoscale Adv.*, 2026, **8**, 532

Novel synthesis of positively charged N,S-doped carbon dots as an efficient fluorescent probe for L-aspartic acid sensing

Ananya Dutta,[a] Dinesh Kumar Shukla[b] and Sonit Kumar Gogoi *[a]

The surface of carbon dots can be easily modified by doping with heteroatoms to tune their optical properties. Hydrothermal treatment of molecular precursors is one of the most useful ways for heteroatom doping. Here, we have developed a novel strategy to dope carbon dots with heteroatoms by the hydrothermal reaction of the nonmolecular, sub-100 nm precursor, carbon powder with L-cysteine. The synthesized carbon dots, N,S-CDs, are positively charged and exhibit an excitation-dependent blue fluorescence (FL). Their average particle size is 1.77 nm, and their average fluorescence lifetime is 2.63 ns, with a fluorescence quantum yield of 25.14%. The N,S-CDs possess good photostability, and the effect of pH on their FL behavior is also studied. The N,S-CDs act as a selective and sensitive fluorescent probe for the detection of L-aspartic acid in aqueous media, and the limit of detection is found to be 2 nM. Fluorescence quenching occurs through the combination of static as well as dynamic paths.

Received 6th August 2025
Accepted 15th November 2025

DOI: 10.1039/d5na00747j

rsc.li/nanoscale-advances

1. Introduction

It has been more than twenty years since the first report on carbon nanoparticles, which came out in 2004, later referred to as carbon dots (CDs) to indicate their high carbon content and zero dimensionality.[1,2] Since then, they have attracted considerable attention, primarily due to their bright, visible light luminescence and ease of synthesis. Their bright and tunable fluorescence (FL), high photostability, water solubility and biocompatibility have outlined CDs as a feasible alternative to metal-based quantum dots.[3,4] Variations in precursors,[5,6] reaction conditions,[7–9] post-synthetic modifications,[10,11] *etc.* are being explored to achieve tailored properties of CDs. Doping with heteroatoms is a promising possibility in this aspect. Wang *et al.*, for the first time, reported the doping of CDs with nitrogen[12] *via* the acid-catalyzed reaction of glycerol and melamine at elevated temperatures to get a high FL quantum yield of 22%. Since then, to control or refine chemical, optical and electrical properties, top-down or bottom-up synthetic approaches for the synthesis of heteroatom-doped CDs have been explored.[12–15] Nonmetal heteroatoms, when doped into CDs, change the electronic structure of the carbon core as well as incorporate multiple surface states, which in turn alter the properties from the undoped ones,[16] and these CDs possess either negative or positive surface charges.[16–21] Consequently, CDs have been used in diverse fields of application including FL sensing,[5,6,22] bioimaging,[23,24] optical devices,[25,26] catalysis,[14,27] and drug delivery.[28,29]

Herein, we propose a novel synthetic strategy for the preparation of nitrogen- and sulfur-doped CDs. We used a carbon-rich non-graphitic reagent obtained through the carbonization of sucrose, *i.e.*, carbon powder,[30] as one of the precursors with the aim of doping it with nitrogen and sulfur from a small organic molecule, L-cysteine. Through a hydrothermal route, the carbon powder is reacted with L-cysteine at different stoichiometric ratios to obtain the nitrogen- and sulfur-doped CDs (N,S-CDs).

Commonly, nonmetal heteroatom-doped CDs are synthesized from small organic molecules with the target heteroatom through pyrolysis, solvothermal treatment, and microwave irradiation.[5,6,18,24,25] Apart from small organic molecules, large biomolecular precursors are also used for the preparation of CDs.[31–33] However, in this novel approach, we have used a two-precursor system, with one of the precursors being carbon-rich (~64.5 at%) and the other precursor, L-cysteine, being the source of the heteroatoms. This enables us to study the influence of doping in a way similar to that of inorganic solids. Here, the carbon-rich precursor acts as the host (similar to an inorganic solid), with the heteroatom originating from the small organic molecule L-cysteine. Through the hydrothermal treatment of the precursors, heteroatom-doped CDs are obtained.

To the best of our knowledge, this is the first report on the heteroatom doping of CDs using a nonmolecular precursor with a small organic molecule *via* hydrothermal treatment.[34–37] We have tabulated a few recent works[38–43] on nonmetal heteroatom-doped (N,S-doped) CDs, along with their precursors and synthetic methods, for comparison in Table 1.

[a]*Department of Chemistry, Gauhati University, G. B. Nagar, Guwahati, 781014, Assam, India. E-mail: skgogoi@gauhati.ac.in*
[b]*UGC-DAE Consortium for Scientific Research, Indore, 452001, India*

Table 1 Nonmetal heteroatom-doped CDs and their synthetic methods

CDs	Doped heteroatom	Precursors	Synthetic method	Reference
CG-CDs	N,S	Citric acid, glutathione	Microwave-induced pyrolysis	38
B-CDs	N,S	Tartaric acid, 1-amino-2-naphthol-4-sulfonic acid	Hydrothermal	39
N,S-CDs	N,S	Ammonium citrate, DL-methionine	Hydrothermal	40
N,S-CDs	N,S	Dithioacetamide, 4-aminophenol	Hydrothermal	41
f-CDs	N,S	Citric acid monohydrate, 4-pyridinecarboxaldehyde, thiourea	Microwave irradiation	42
CDs	N,S	Polyvinylpyrrolidone, citric acid, methionine	Hydrothermal	43

Amino acids are the building blocks of protein, which comprises nearly half of the dry weight of a mammalian body.[44] The concentration of amino acids in the body of a diseased person varies from that in a healthy individual, and such differences can be used as biomarkers for the diagnosis and monitoring of various diseases.[44–50] The essential amino acid glycine plays a major role in glucogenesis as well as in the secretion of glucagon and insulin, whose reduced level in the body acts as a biomarker for prediabetes, insulin resistance, and early type 2 diabetes.[45] Aspartic acid is a serum amino acid, which, along with being a major precursor for the synthesis of glycine and glutamic acid, plays an important role in the Krebs cycle.[46] In the case of clear cell renal cell carcinoma (ccRCC) patients, the concentration of aspartic acid in the patient's body becomes higher (28.95 ± 4.03 μmol L^{-1}) than that in a healthy individual's body (2.69 ± 1.07 μmol L^{-1}); variations in the concentration of other amino acids are also observed *via* amino acid profiling.[47] An excess of aspartic acid in the body can cause Lou Gehrig's disease,[48] which is associated with the early onset of Alzheimer-type dementia.[49,50] Abnormal levels of aspartic acid in the body can also be used as a marker for epilepsy, osteoarthritis, *etc.*[50] This crucial role of amino acids in our body has encouraged researchers to develop various experimental techniques like chemical oscillatory systems, chiral ligand exchange capillary electrophoresis, ion exchange chromatography, HPLC, LCMS, potentiometry, and FL and colorimetric detection for the detection of amino acids.[48–56] Due to the ease and cost-effectiveness of FL-based detection, CDs have also been used as FL probes for the detection of amino acids.[48,50,54–56]

The synthesized blue-fluorescent N,S-CDs are positively charged with an FL quantum yield (FLQY) of 25.14%. N,S-CDs can selectively detect L-aspartic acid in aqueous media through FL quenching by the combination of static and dynamic mechanisms, with a limit of detection (LOD) of 2 nM.

2. Experimental

2.1 Materials

Sucrose and sodium hydroxide were purchased from Merck, India, and concentrated sulfuric acid and hydrochloric acid from Qualigens were used. L-Cysteine (Cys) and valine (Val) were purchased from Himedia. L-Alanine (Ala), L-arginine (Arg), L-glycine (Gly), L-aspartic acid (L-asp), L-leucine (Leu), L-histidine (His), L-lysine (Lys), L-tryptophan (Trp), L-tyrosine (Tyr), L-glutamic acid (Glu), L-proline (Pro), L-methionine (Met), L-serine (Ser), L-threonine (Thr) and phenylalanine (Phe) were purchased from SRL. Quinine sulfate was purchased from Loba Chemie. For all the experiments, double-distilled water from an EQUITRON distilled water setup was used.

2.2 Characterization

The powder X-ray diffraction patterns of the samples were recorded from $2\theta = 5°$ to 80° using a Rigaku Ultima IV instrument with Cu Kα radiation ($\lambda = 1.54$ Å) at room temperature. The morphology and elemental composition of the carbon powder were studied by FESEM (Zeiss, Sigma 300) and EDAX (Amtek), respectively. The morphologies of N,S-CDs were observed using a high-resolution transmission electron microscope (FP 5022/22-Tecnai G2 20 S-TWIN, USA). Their particle size distribution was observed through dynamic light scattering (DLS), and the surface charge of the nanoparticles was measured using a zeta sizer (Nano ZS90, Malvern Analytical) and a NICOMP zeta potential instrument (Z3000, ZW388 software), respectively. The X-ray photoelectron spectrometry (XPS) spectra of the drop-casted samples were recorded with a SPECS ESCA spectrometer (Germany). As per the specifications of the ESCA spectrometer, 1 eV was subtracted from each binding energy value obtained for charge correction. The elemental analysis and mapping of the samples were carried out using the EDAX by Ametek. FTIR spectra were recorded using SHIMADZU IR Affinity-1. The spectral measurement of UV-visible absorption was performed using a UV-1800 spectrophotometer (SHIMADZU, Japan). A Hitachi FL spectrophotometer (F-7000) was used to record FL spectra. FL lifetimes were recorded using a picosecond lifetime spectrophotometer (Lifespec II, Edinburgh Instruments). The visual inspection of FL was done using a UV inspection cabinet. To check the pH, a waterproof pH meter (PH-035, ERMA Inc.) was used.

2.3 Synthesis of N,S-CDs

Through a hydrothermal reaction of the carbon powder (acid carbonization product of sucrose)[30] with Cys, CDs were synthesized. The amount of the carbon powder was kept constant at 0.1 g, whereas the amount of Cys was varied from 0.1 g to 0.7 g to obtain 1 : 1, 1 : 3, 1 : 5 and 1 : 7 ratios. In each case, the reaction mixture of the specific ratio was dispersed in 20 mL of distilled water, transferred to a 150 mL Teflon-lined stainless-steel autoclave and heated at 230 °C for 6 hours in a laboratory oven. The autoclave was cooled to room temperature, and an orange-colored liquid mixture was obtained. This mixture was centrifuged at 10 000 rpm for 40 minutes to remove

large particles, and the supernatant was collected. The dilute aqueous dispersion of this supernatant was colorless under normal room light and was used for further analysis. Out of all the reaction conditions, the products obtained at a 1 : 3 ratio exhibited the highest FL intensity and quantum yield (QY) when recorded under identical conditions (Fig. S1(a) and (b)). So, this product, designated as N,S-CDs, was used in all analyses. The properties of the carbon powder were also studied during the course of the work.

2.4 Quantum yield determination

The FLQYs of the synthesized N,S-CDs and the products obtained from the reactions of precursors at different stoichiometric ratios were measured by the relative quantum yield determination method, considering quinine sulfate in 0.1 mol L^{-1} H_2SO_4 ($\phi = 0.54$) as the standard. Eqn (1), given below, was used for the calculation of the quantum yield:

$$\phi_X = \phi_{ST} \times (G_X/G_{ST}) \times (\eta_X{}^2/\eta_{ST}{}^2) \quad (1)$$

where G is the gradient of the plot, η is the refractive index of the solvent, and ϕ is the quantum yield; 'X' refers to CDs, and 'ST' refers to quinine sulfate (refractive index = 1.33). The FLQY was found to be the maximum for N,S-CDs (25.14%) (Fig. S1, Table S1).

2.5 Stability of N,S-CDs and effect of pH

The stability of the FL behavior of the synthesized N,S-CDs was checked by putting them in different molar concentrations of NaCl. By keeping the N,S-CDs under UV irradiation for different time intervals, their photostability was also checked. Besides, the effect of acidic and basic media on the FL behavior of N,S-CDs was studied by varying the pH of the sample solution.

2.6 FL sensing of L-asp

A stock solution was prepared by dispersing 50 μL of N,S-CDs in 200 mL of distilled water. For the L-asp sensing experiment, to 2 mL of an N,S-CD dispersion, different concentrations (50 μM to 0.1 nM) of 10 μL of an L-asp solution were added, and the FL emission spectrum of each of the mixtures was recorded at a 320 nm excitation wavelength at room temperature, keeping both excitation and emission slits at 5 nm.

2.7 Selectivity test

The selectivity of N,S-CDs for L-asp was compared with that for other amino acids such as Ala, Arg, Gly, Leu, His, Lys, Trp, Tyr, Cys, Glu, Pro, Met, Ser, Thr, Phe and Val by recording the FL emission spectra under identical conditions. The concentration of L-asp and other amino acids considered was 50 μM.

3. Results and discussion

3.1 Characterization

The broad peak at 18.5° in the PXRD pattern of the carbon powder can be assigned to the (002) plane of graphitic layers with an interplanar/interlayer spacing of 0.48 nm (Fig. S2(a)). However, this is larger than the interlayer spacing of pure graphite (0.34 nm),[57] indicating its amorphous nature and incomplete graphitization, which leaves oxygenated functional groups, as confirmed by the EDX and FTIR spectroscopy results discussed later. The presence of oxygenated functional groups, similar to those in graphene oxides, leads to the larger interlayer spacing than that of graphite.[58] The FESEM image of the carbon powder (Fig. S2(b)) indicates the presence of sub-100 nm particles in the majority of the system. The size, measured using the ImageJ software, indicates that sub-100 nm particles mostly have a size in the range of 70–90 nm, and a few larger particles with a size in the range of 110–128 nm are also present. The EDX spectrum of the carbon powder has carbon (64.5 at%) as the major component along with oxygen (35.15 at%) and traces of sulfur (0.11 at%) (Fig. S2(c)). The trace amount of gold in the EDX spectrum is due to the gold coating.

Heteroatom doping is a convenient method for surface modification and tuning the electronic properties of CDs so that better/tunable optical properties are attained.

The size of N,S-CD particles, imaged by TEM (Fig. 1(a)) and analyzed using the ImageJ software, is found to be in the 1.13 nm to 3 nm range (Fig. 1(b)), with an average particle size of 1.77 nm. Corroborating results from DLS measurements show that about 58% of the particles have a size of 1.49 nm (Fig. 1(c)) with a relatively narrow size distribution. The broad peak centered at 23.5° in the PXRD pattern of N,S-CDs can be indexed to the (002) plane of graphitic carbon[59] with an interplanar spacing of 0.38 nm (Fig. 1(d)) slightly larger than the interlayer spacing of graphite (0.34 nm).[57] Upon comparison with the PXRD results of the carbon powder, a greater degree of graphitization is evident for N,S-CDs due to the hydrothermal process.

The surface charge of N,S-CDs is found to be +3.44 mV from zeta potential measurements (Fig. S3). The EDX spectroscopic analysis (Fig. 2(a)) shows that the at% of carbon, nitrogen, oxygen and sulfur in N,S-CDs is 60.19%, 8.17%, 27.01% and 4.34%, respectively, with a uniform surface distribution of these elements in N,S-CDs; elemental mapping is shown in Fig. S4.

The surface functional moieties in N,S-CDs are determined by FTIR spectroscopic and XPS techniques. The FTIR spectra of the carbon powder and N,S-CDs are shown together in Fig. 2(b). In the carbon powder, the peak at 1620 cm^{-1} corresponds to the C=C stretching vibration of the graphitic skeleton.[60] The peaks at 1452 cm^{-1} and 1020 cm^{-1} are attributed to the C–H bending vibration and stretching vibration of the epoxy group, respectively.[61,62] The weak peak at 1184 cm^{-1} is due to the symmetric stretching of the $-SO_3H$ group,[63] which might be because of the traces of sulfur present in the sucrose used for the preparation of the carbon powder. The peak at 760 cm^{-1} is due to the aromatic C–H out-of-plane stretching vibration.[62] In the FTIR spectrum of N,S-CDs, absorption bands corresponding to oxygen-, nitrogen- and sulfur-containing functional groups are observed. The broad peak at 3436 cm^{-1} corresponds to the –OH/N–H stretching vibration.[64] The peaks at 2120 cm^{-1} and 1620 cm^{-1} are attributed to S–H and C=C stretching vibrations, respectively.[60] The peak at 1108 cm^{-1} corresponds to $-SO_3H$

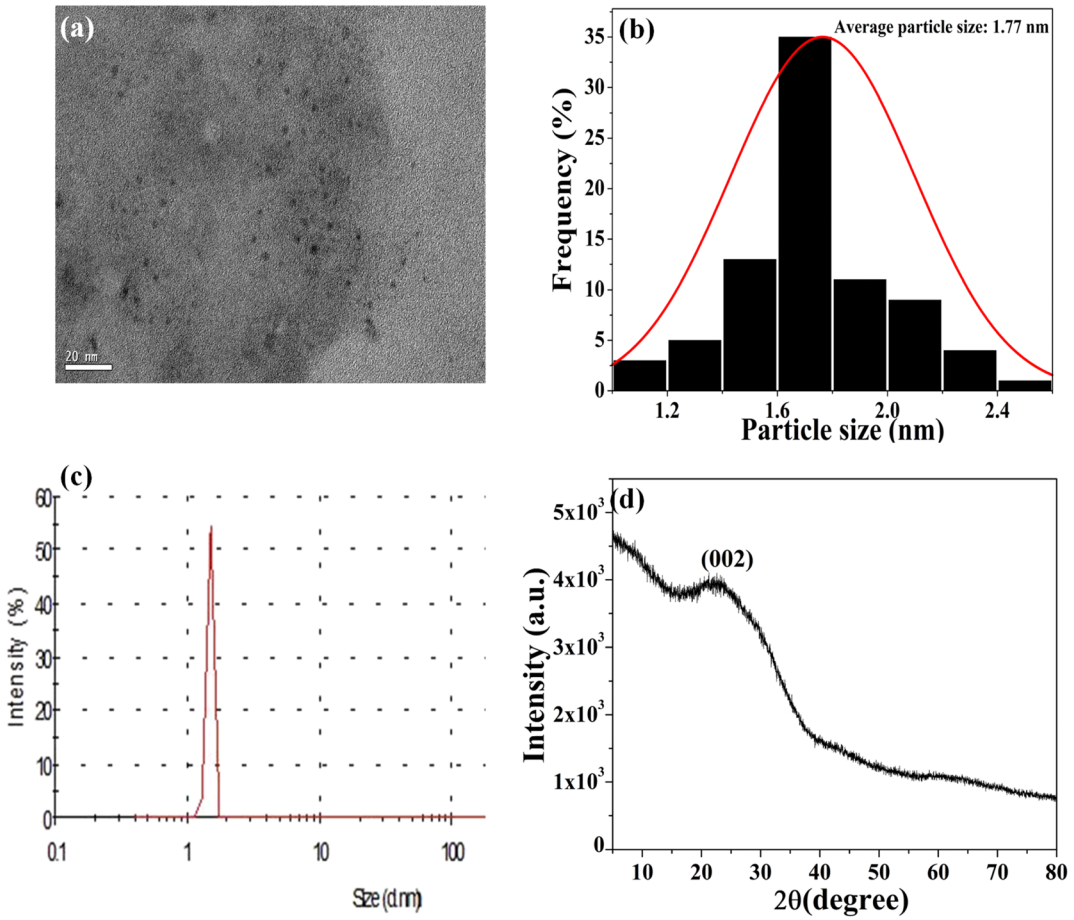

Fig. 1 (a) TEM image, (b) particle size distribution determined from TEM imaging, (c) DLS particle size distribution, and (d) powder X-ray diffraction pattern of N,S-CDs.

stretching vibrations, and that at 624 cm^{-1} corresponds to C–S stretching vibrations.[65]

In the XPS survey spectrum (Fig. 2(c)) four peaks at 159 eV, 286.5 eV, 401 eV and 533 eV are observed, corresponding to the binding energies of S 2p, C 1s, N 1s and O 1s, respectively.[66–68] The high-resolution XPS spectra are deconvoluted to a number of individual peaks for the elements present (Fig. 2(d)–(g)). The four peaks at 285.02 eV, 286.93 eV, 288.46 eV and 290.15 eV for C 1s (Fig. 2(d)) are assigned to C–S/C=C, C–N/C–O, O–C=O and C=O groups, respectively.[69,70] Similarly, for N 1s (Fig. 2(e)), the three peaks at binding energies of 400.7 eV, 401.8 eV and 402.9 eV are attributed to C–NH_2 and pyridinic and pyrrolic N groups, respectively, indicating nitrogen doping in the graphitic structure.[71,72] The presence of the amine groups on the surface leads to the positive surface charge when protonated, correlating well with the +4.33 mV surface charge observed for the N,S-CDs in the zeta potential measurements (Fig. S3). The high-resolution O 1s spectrum, upon deconvolution, gives four peaks (Fig. 2(f)). The peak at 532.1 eV is due to the C–OH group.[71] The peaks at 533.2 eV and 534.4 eV are ascribed to the O=C–O group.[72,73] The weak peak at 536.2 eV is attributed to trapped moisture.[74] The high-resolution S 2p spectrum (Fig. 2(g)) is deconvoluted into two peaks centered at 164.9 eV and 169.8 eV, respectively. The binding energy peak at 164.9 eV is attributed to the $2p_{1/2}$ state of C–S–C, whereas the peak at 169.8 eV is due to the presence of C–SO_x species ($x = 2$–4) in N,S-CDs.[75] The presence of the polar functional groups on the surface makes N,S-CDs well dispersible in water.

3.2 FL properties of N,S-CDs

An overview of the optical properties of N,S-CDs was obtained from the UV-visible absorbance, FL and FL excitation (FLE) spectra of N,S-CDs (Fig. 3(a)). In the UV-visible spectrum, black line in Fig. 3(a), there is a weak peak at 236 nm and two shoulder peaks at 270 nm and 310 nm. The peaks at 236 nm and 270 nm are due to the π–π* transition, whereas the *n*–π* transition related to the nonbonding electrons on heteroatom-containing groups gives the 310 nm absorption peak.[76,77] A broad emission peak centered at 396 nm is observed upon excitation at 320 nm, red line in Fig. 3(a). The N,S-CDs exhibit blue fluorescence; Fig. S5(a) shows the photographs of N,S-CDs under white light and a 365 nm UV lamp. The corresponding chromaticity diagram (Fig. S5(b)) confirms the observation of blue fluorescence.[78] The fluorescence excitation (FLE) spectrum comprises three peaks centered at 238 nm, 275 nm and 323 nm, blue line in Fig. 3(a), similar to the UV-visible absorption spectrum. The higher intensity of the peak at

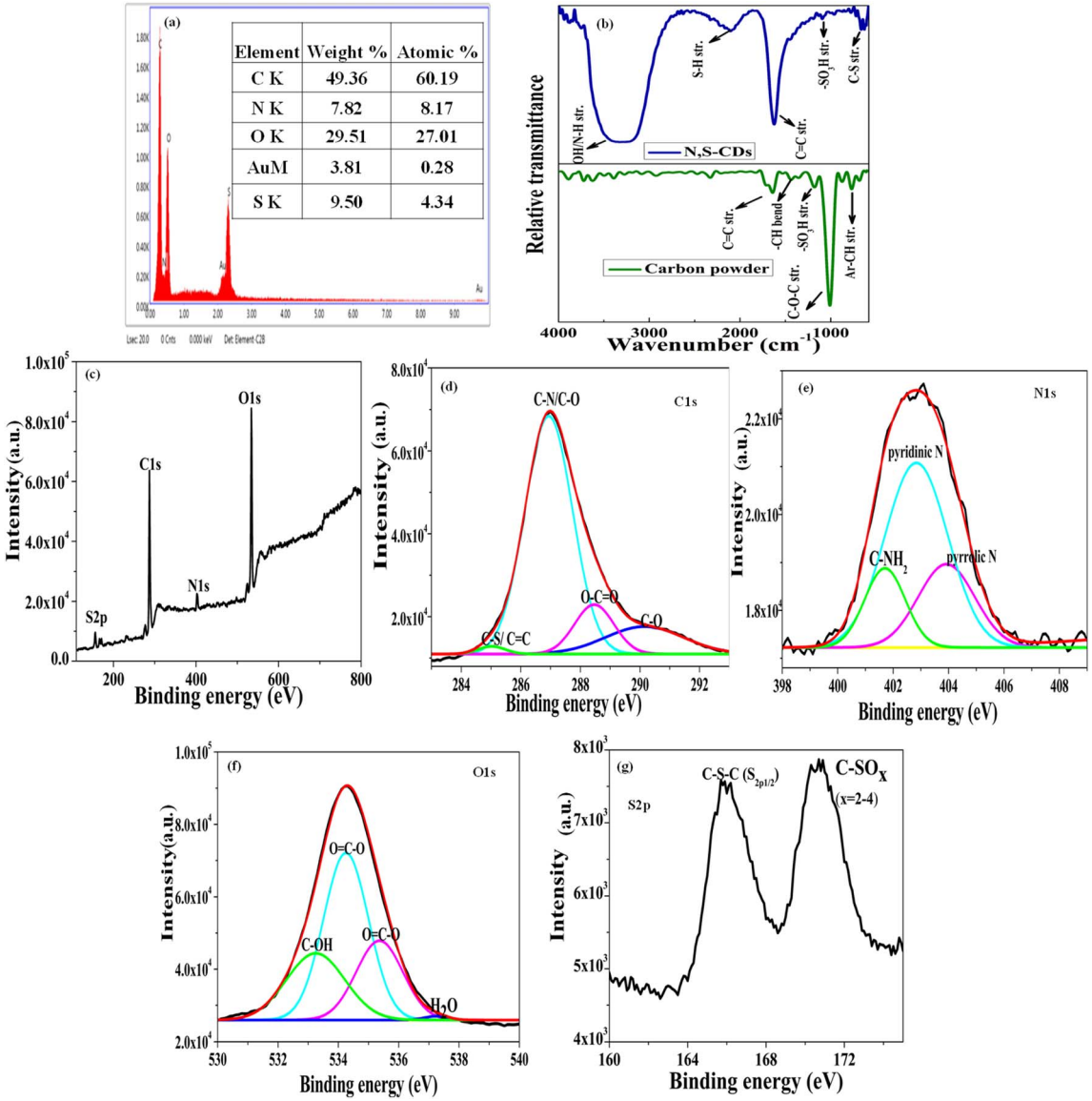

Fig. 2 (a) EDX spectrum, (b) combined FTIR spectra, (c) XPS survey spectrum, and high-resolution XPS spectra of (d) C 1s, (e) N 1s, (f) O 1s and (g) S 2p of N,S-CDs.

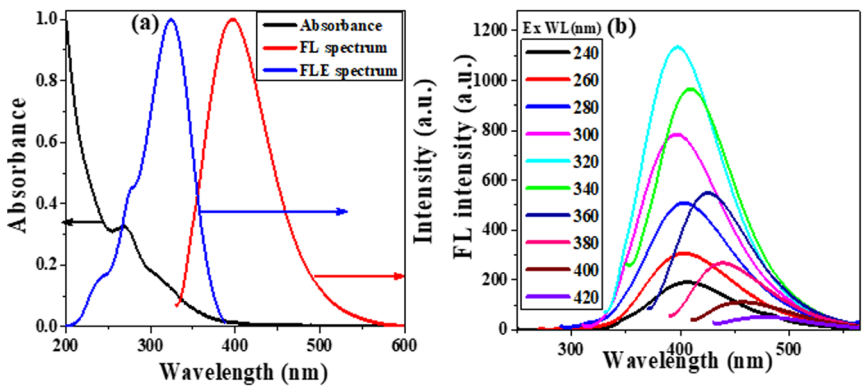

Fig. 3 (a) UV-visible absorption spectrum (black), FL emission spectrum (red) and FLE spectrum (blue) of N,S-CDs. (b) FL emission spectra of N,S-CDs at varying excitation wavelengths.

323 nm in the FLE spectrum indicates that the n–π^* state makes a major contribution towards the FL emission centered at 396 nm. The FL emission spectrum of N,S-CDs in the excitation wavelength range from 240 nm to 420 nm (Fig. 3(b)) shows an emission center shift from 406 nm to 474 nm, with the emission maximum at 396 nm after 320 nm excitation, characteristic of luminescent CDs.

The FL behavior of the synthesized N,S-CDs is different from that of its precursors, carbon powder and Cys, and that of the products obtained *via* the hydrothermal treatment of each of the precursors alone under the same reaction conditions (Fig. S6(a)). The carbon powder and its hydrothermal treatment product have an FL emission center at the same position, 386 nm after 320 nm excitation. However, the hydrothermal reaction product of the carbon powder shows a higher FL intensity than the carbon powder, which can be attributed to the formation of CDs, as also indicated by the broad PXRD diffraction peak observed in Fig. S6(b). Similarly, the FL emission of Cys hydrothermally treated at 230 °C shows an emission centered at 383 nm, with its PXRD pattern different from that of molecular Cys. Hence, it can be said that the hydrothermal product of Cys, which could not be identified at this stage, is different from its precursor with some degree of FL emission. However, the emission center of the hydrothermal product of Cys lies at 383 nm for the same excitation wavelength, while that of N,S-CDs lies at 396 nm (Fig. S6(a)), and a PXRD pattern similar to those of most CDs reported in the literature[7,8,67,71] is observed for N,S-CDs (Fig. S6(b)). Besides, the FL intensity is found to be the maximum for N,S-CDs among the carbon powder, the carbon powder hydrothermally treated at 230 °C for 6 h, Cys hydrothermally reacted at 230 °C for 6 h, and N,S-CDs at a 320 nm excitation wavelength (Fig. S6(a)). Thus, the N,S-CDs are different from all of the precursors as well as the products of hydrothermal treatment of any one of the precursors alone. The incorporation of the heteroatoms N and S into the carbon powder system results in the higher FL intensity of N,S-CDs compared to that of the rest (Fig. S6(a)).

The N,S-CDs, a product of the hydrothermal treatment of the carbon powder : Cys at a 1 : 3 ratio, show the highest emission intensity and FLQY compared to the products at other ratios (Fig. S1 and Table S1). This can be related to the extent of CD formation during the formation of the final product, as evident from their PXRD pattern (Fig. S7). The PXRD analysis of the hydrothermal products shows the formation of higher amounts of CDs at the ratios of 1 : 3 and 1 : 5. During the formation of nitrogen- and sulfur-doped CDs, Cys reacts with the carbon powder to introduce sulfur and nitrogen with a simultaneous reduction in the size, as shown in the FESEM and TEM images in Fig. S2(b) and 1(a). For instance, in the PXRD pattern of the product with the 1 : 5 ratio of carbon powder and Cys (second highest QY among all the products, 22.58%), along with a broad peak at $2\theta = 23.5°$ for the (002) plane, a sharp peak at a 2θ value of about 9°, corresponding to the (006) plane of L-cystine,[79] is observed, which indicates that the unreacted L-cystine present in the final product blocks some of the radiative emissive sites present on the CDs, leading to a lower FL intensity and FLQY than to those of N,S-CDs. L-Cystine and Cys are not fluorescent; so, their presence in the product can perturb the extent of possible radiative emission. When 1(carbon powder) : 1 (Cys) and 1(carbon powder) : 7(Cys) products are synthesized, there is a possibility of incomplete condensation of the precursors, resulting in some peaks corresponding to Cys and unknown hydrothermal products in the PXRD pattern (Fig. S7). Such crystalline peaks also indicate incomplete carbonization during the formation of the final product, leaving behind nonfluorescent moieties in the products to bind with the radiative emission sites, which are responsible for the observed decrease in the FL intensity and FLQY. The unchanged position of the FL emission center for all ratios at a 320 nm excitation wavelength clearly depicts that the remaining nonfluorescent moieties, which block some of the emissive sites, are the reason behind the decreased FL intensity as well as FLQY.

From the PXRD and FL observations, we can say that although doping can lead to better FL behavior in CDs, carbonization is the most crucial step for the observed FL behavior of CDs.

3.2.1 Effect of the pH, ionic strength, photostability and colloidal stability on the FL behavior of the N,S-CDs. The pH of the aqueous dispersion of the synthesized N,S-CDs is 6.9. To check the effect of varying pH on the FL behavior of N,S-CDs, their UV-visible absorption spectra and FL emission spectra at a 320 nm excitation wavelength were recorded, as shown in Fig. 4(a) and (b), respectively.

With lowering pH from 6.9 to 2.6, a minimal decrease in the absorbance (Fig. 4(a) and FL intensity (Fig. 4(b)) is observed. As the N,S-CDs are already positively charged, the addition of excess H^+ ions *via* the lowering of pH has little effect on their absorbance and emission. Whatever little quenching of the FL emission observed can be attributed to the protonation of emissive surface sites on the N,S-CD surface. The oxygenated functional moieties on the surface can be protonated in such situations. However, under alkaline conditions, with an increase in the pH from 6.9 to 12.4, a considerable decrease in the absorbance (Fig. 4(a)) and FL intensity (Fig. 4(b)) is observed. In the absorbance spectrum (Fig. 4(a)), the 270 nm π–π^* peak and 310 nm n–π^* peak have lower absorbance at higher pH compared to that at the pH 6.9 of the stock solution of N,S-CDs, with no change in the relative peak intensities of these two peaks. As the pH is on the alkaline side, the deprotonation of the surface functional groups of N,S-CDs is expected, leading to a reduction in the positive surface charge on N,S-CDs. With reduced positive surface charges, there may be agglomeration of N,S-CDs, resulting in the removal of particles from the dispersion by precipitation, and consequently, a reduction in the absorbance (Fig. 4(a)) and FL intensities (Fig. 4(b)) is observed.

The effect of the ionic strength on the FL behavior of N,S-CDs was studied by adding NaCl solutions of different molar concentrations (Fig. 4(c)). It is observed that the FL intensity of N,S-CDs shows very little change upon the addition of NaCl solutions of concentrations up to 1.5 M. Because salt water contains 1.5 M NaCl, we can say that the synthesized N,S-CDs retain their FL behavior in salt water as well. The FL behavior of N,S-CDs was also observed after irradiation under a 365 nm UV lamp for different time intervals up to 60 min (Fig. 4(d)). No significant change in the FL intensity with these irradiation times indicates the high photostability of N,S-CDs.

To assess the colloidal stability of the aqueous N,S-CDs, they were kept under ambient conditions for 7 days, and their FL

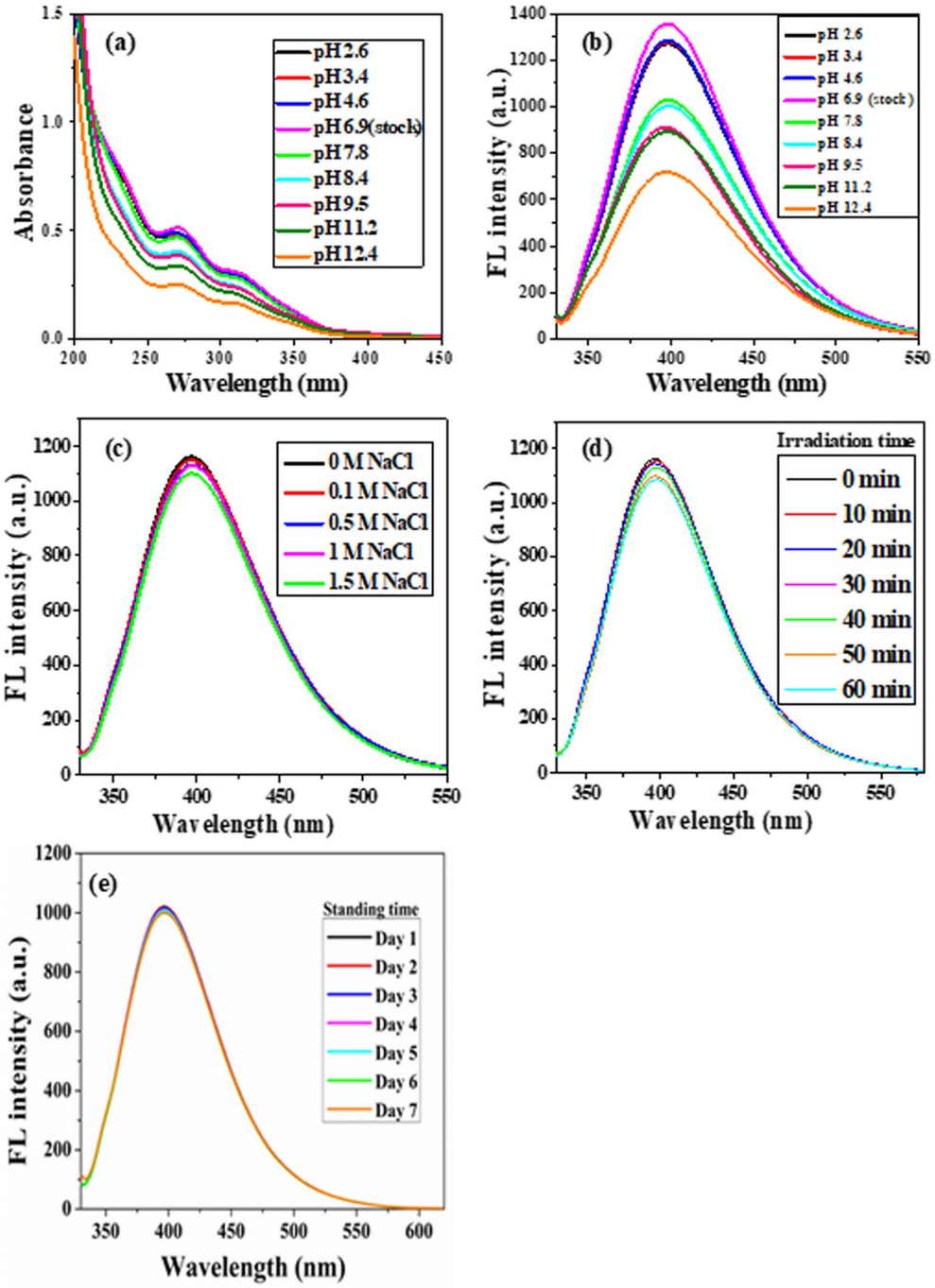

Fig. 4 (a) UV-visible absorption spectra (b) FL emission spectra at different pH, (c) FL emission spectra at different NaCl concentrations, (d) FL emission spectra after different duration of UV irradiation and (e) FL emission spectra recorded upto 7 days under ambient conditions of N,S-CDs.

emission spectra were recorded each day. No change in the FL intensity or the emission center is observed (Fig. 4(e)) for up to 7 days, indicating good colloidal stability.

3.2.2 FL sensing of L-asp. Owing to the stable emission of N,S-CDs, we have employed them as an FL probe for the detection of L-asp. The selectivity of N,S-CDs towards L-asp was checked by adding 10 μL of 50 μM aqueous solutions of amino acids (Ala, Arg, Gly, Leu, His, Lys, Trp, Tyr, Cys, Glu, Pro, Met, Ser, Thr, Phe, and Val) to 2 mL of an N,S-CD dispersion. Only upon the addition of L-asp does visible quenching of the FL intensity of N,S-CDs occur, whereas no such quenching is observed for other amino acids recorded at an excitation wavelength of 320 nm (Fig. 5(a)). The corresponding bar graph with error bars (Fig. 5(b)), plotted from three sets of replicate measurements, also clearly shows the selectivity of N,S-CDs towards L-asp. To check the sensitivity of the N,S-CD system towards L-asp in aqueous dispersions, the FL emission spectra of N,S-CDs were recorded over a wide concentration range of L-asp, ranging from 0.1 nM to 50 μM

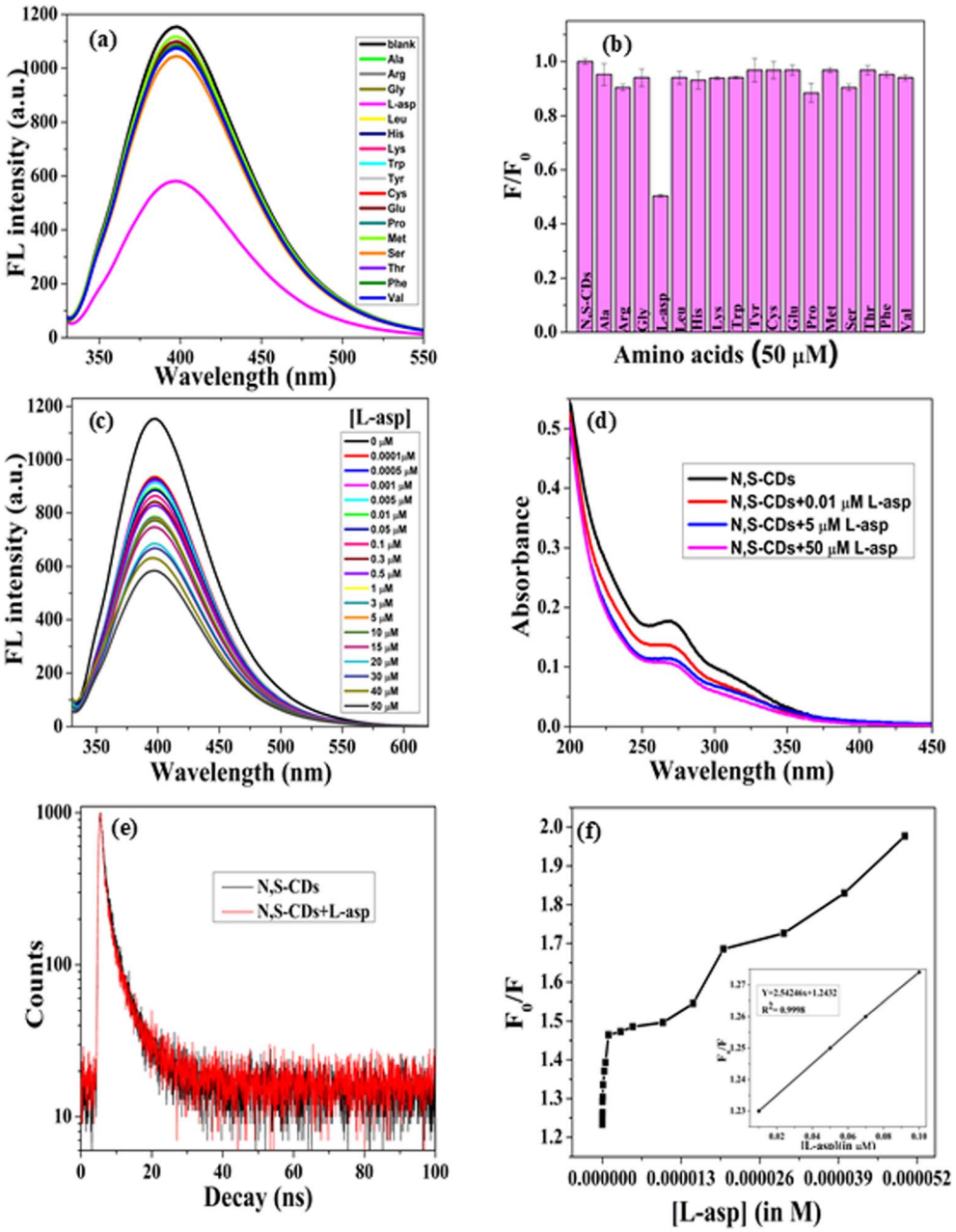

Fig. 5 (a) FL spectra of N,S-CDs in the presence of amino acids under consideration (50 μM at a 320 nm excitation wavelength), (b) corresponding bar graph with error bars, (c) FL emission spectra of N,S-CDs in the presence of different L-asp concentrations, (d) UV-visible absorption spectra of N,S-CDs in the presence of L-asp, (e) FL lifetime plot of N,S-CDs alone and in the presence of L-asp, and (f) F_0/F *vs.* concentration plot for the complete range of the L-asp concentration studied (inset: F_0/F *vs.* L-asp concentration plot for the concentration range from 0.001 μM to 0.01 μM).

(Fig. 5(c)). Upon the addition of L-asp concentrations as low as 0.1 nM, the FL intensity of N,S-CDs is quenched by 18.84%. With an increase in the concentration of L-asp, the quenching of the FL emission signal increases. For 50 μM L-asp, there is 49.39% quenching of the FL intensity of N,S-CDs. A gradual decrease in absorbance is observed in the UV-visible absorption spectrum of N,S-CDs with an increase in the L-asp concentration (Fig. 5(d)). Also, a decrease in the FL lifetime of N,S-CDs from 2.63 ns to 1.85 ns is observed after the addition of L-asp (Fig. 5(e)). The F_0/F *vs.* $[Q]$ plot (Fig. 5(f)) shows a complicated behaviour with a deviation from the regular linear Stern–Volmer plot. Upon close inspection (Fig. S8(a) and (b)), one can observe the negative deviation of the F_0/F *vs.* $[Q]$ plot in the concentration range from 0.0001 μM to 0.5 μM and an exponential change in the range from 1 μM to 50 μM, respectively. The negative deviation in the F_0/F *vs.* $[Q]$ plot (Fig. S8(a)) is related to the presence of multiple fluorophores with different accessibilities to the quencher molecule, thus leading to the quenching of one of the fluorophores and no quenching or partial quenching of the other fluorophores due to the limited access to the quencher molecule L-asp. The exponential fit (Fig. S8(b)) in the higher-concentration range, 1 μM to 50 μM, in

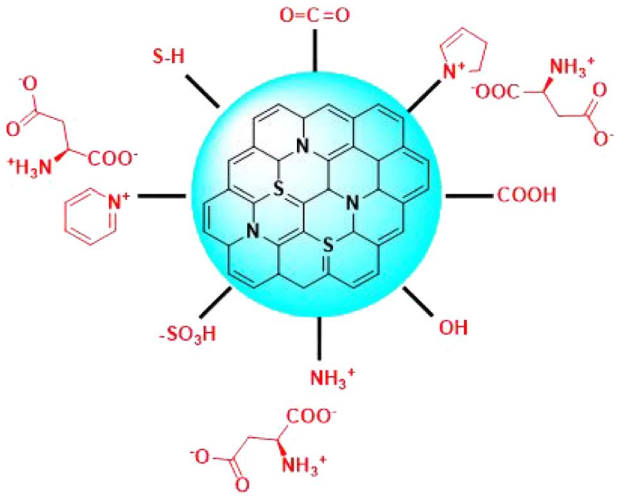

Scheme 1 Plausible way for the interaction of N,S-CDs with L-asp.

the F_0/F *vs.* [Q] plot can be related to the modified Stern–Volmer relation given below:

$$\frac{F_0}{F} = (1 + K_{SV}[Q])e^{V[Q]} \quad (2)$$

where V represents an active volume surrounding the excited fluorophore. The exponential component $e^{V[Q]}$ gives the involvement of a static association of the quencher molecule, in this case, L-asp, with the excited fluorophore, N,S-CDs, when within the active volume of interaction.[80]

Aspartic acid in aqueous media can interact electrostatically with the positively charged or protonated surface sites of N,S-CDs to form a nonfluorescent ground-state adduct, Scheme 1. This is evident from Fig. 5(d), which shows the decrease in the UV-visible absorbance of the N,S-CD system in the presence of L-asp, accounting for the static component in the observed FL quenching. The change in the zeta potential of N,S-CDs from +3.44 mV (Fig. S3) to +1.13 mV (Fig. S8(c)) for the N,S-CDs-L-asp adduct is indicative of the said electrostatic interaction.

By contrast, the decrease in the FL lifetime of N,S-CDs upon the addition of L-asp (Fig. 5(e)) indicates the dynamic component in FL quenching. There are three possibilities for the excited-state process in FL quenching: the inner filter effect (IFE), Förster resonance energy transfer (FRET) and photoinduced electron transfer (PET). For the IFE and FRET to occur, the FL spectrum of the fluorophore (probe N,S-CDs) should overlap with the absorbance spectrum of the quencher (analyte L-asp). In the UV-visible absorbance spectrum of L-asp and the FL emission spectrum of N,S-CDs, when plotted together (Fig. S8(d)) no such coverage is observed, indicating that neither IFE nor FRET is involved in the quenching phenomenon. By contrast, for the short-range PET process, there is no such requirement.[81] So, PET may be the dynamic pathway contributing towards the observed quenching. Because N,S-CDs are positively charged, *i.e.* electron-deficient, in the excited state, they act as an acceptor of electrons donated by the negatively charged aspartate ions (the isoelectric point of L-asp (pI) is 2.98), *i.e.* they can get involved in the process of reductive photoinduced electron transfer (rPET). So, under the experimental pH (6.9) condition, there is a possibility of electron transfer from the HOMO of L-asp to the now-vacant (HOMO at the ground state) molecular orbital of N,S-CDs, leading to dynamic quenching of the FL intensity and a reduction in the lifetime, Scheme 2.[82,83]

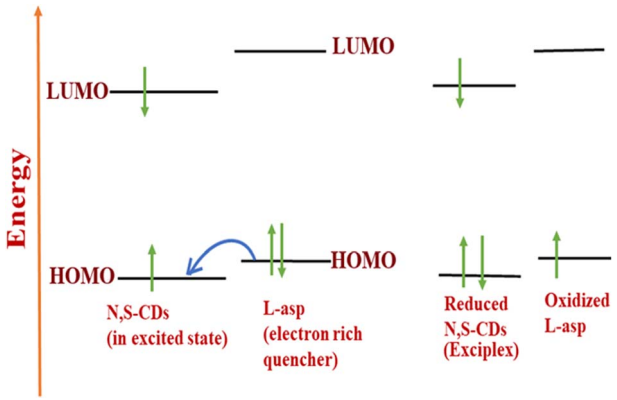

Scheme 2 Schematic of rPET occurring in the N,S-CDs-L-asp system for FL quenching.

The F_0/F *vs.* L-asp concentration plot appears linear at very low concentrations of L-asp, *i.e.*, from 0.001 μM to 0.01 μM, inset in Fig. 5(f). The corresponding linear regression equation is $Y = 2.5098x + 1.2424$ (the value of the correlation constant is $R^2 = 0.99$), and the slope (k) is 2.5098. The residual standard deviation (RSD) is 0.0016. The limit of detection (LOD) is calculated using the equation:

$$\text{LOD} = 3\sigma/s \quad (3)$$

where σ is the RSD and s is the slope of the calibration plot. The limit of detection (LOD) is found to be 2 nM.

The photographs of N,S-CD solutions in the presence of various amino acids are a visual representation of FL quenching in the presence of L-asp (Fig. 6). The blue color of the N,S-CD solution remains unaltered in the presence of all other amino acids under consideration, whereas a visible decrease in the blue color is observed in the presence of L-asp when viewed under 365 nm UV light.

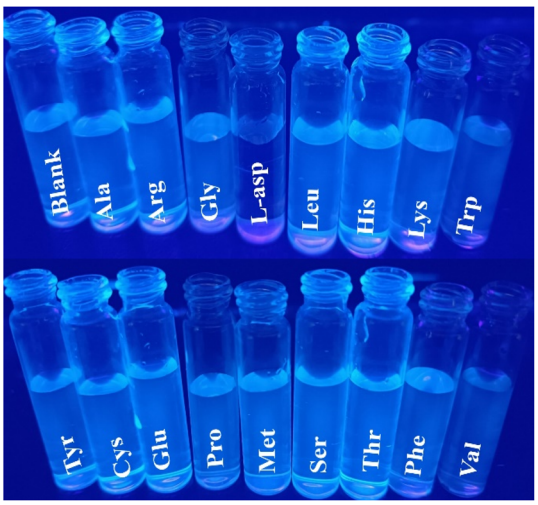

Fig. 6 Photographs of the N,S-CD solutions in the presence of various amino acids under a 365 nm UV light.

4. Conclusion

Using a novel method, by reacting carbon powder with Cys hydrothermally, we have successfully synthesised cationic N,S-CDs. The N,S-CDs have an average size of 1.77 nm with a very narrow range of size distribution. With 60.19% carbon, 8.17% nitrogen, 27.01% oxygen and 4.34% sulfur, N,S-CDs have a zeta potential value of +4.33 mV and have excellent FL stability. Changing the pH of the medium changes the FL intensity of the system without changing the position of the emission maximum. The N,S-CDs exhibit high selectivity and sensitivity in L-asp FL sensing compared to that for all other amino acids in aqueous media. Detailed studies show that both static and dynamic processes are involved in the observed FL quenching, with the limit of detection found to be 2 nM for L-asp.

Author contributions

Ananya Dutta: conceptualization, methodology, synthesis, characterization and application of the materials, writing-original draft, reviewing. Dinesh Kumar Shukla: instrumental analysis. Sonit Kumar Gogoi: supervision, writing-original draft, reviewing, editing.

Conflicts of interest

The authors declare that they have no known competing financial interests or personal relationships that could have had any impact on the work reported in this paper.

Data availability

The data supporting this article have been included as part of the supplementary information (SI). Supplementary information is available. See DOI: https://doi.org/10.1039/d5na00747j.

Acknowledgements

The authors acknowledge SERB-DST SB/S1/PC-105/2012 and UGC-DAE grant CRS/2021-22/01/410 for financial assistance. The authors are also thankful to SAIF, Gauhati University, for extending instrumental support. The authors also express gratitude to the DST-FIST program for the powder XRD facility at the Department of Chemistry, Gauhati University and DST PURSE, Gauhati University, for financial assistance.

References

1 J. Liu, R. Li and B. Yang, *ACS Cent. Sci.*, 2020, **6**, 2179–2195.
2 X. Xu, R. Ray, Y. Gu, H. J. Ploehn, L. Gearheart, K. Raker and W. A. Scrivens, *J. Am. Chem. Soc.*, 2004, **126**, 12736–12737.
3 Y. Liu, H. Huang, W. Cao, B. Mao, Y. Liu and Z. Kang, *Mater. Chem. Front.*, 2020, **4**, 1586–1613.
4 S. Ying Lim, W. Shen and Z. Gao, *Chem. Soc. Rev.*, 2015, **44**, 362–381.
5 M. L. Liu, B. B. Chen, C. M. Li and C. Z. Huang, *Green Chem.*, 2019, **21**, 449–471.
6 X. Zhang, X. Liao, Y. Hou, B. Jia, L. Fu, M. Jia, L. Zhou, J. Lu and W. Kong, *J. Hazard. Mater.*, 2022, **422**, 126881.
7 T. Garcia-Millan, T. A. Swift, D. J. Morgan, R. L. Harniman, B. Masheder, S. Hughes, S. A. Davis, T. T. A. Oliver and M. Carmen Galan, *Nanoscale*, 2022, **14**, 6930–6940.
8 Y. Zhang, Y. Wang, X. Feng, F. Zhang, Y. Yang and X. Liu, *Appl. Surf. Sci.*, 2016, **387**, 1236–1246.
9 Y. H. Yuan, Z. X. Liu, R. S. Li, H. Y. Zou, M. Lin, H. Liu and C. Z. Huang, *Nanoscale*, 2016, **8**, 6770–6776.
10 S. A. Chernyak, A. M. Podgornova, S. G. Dorofeev, S. Maksimov, K. I. Maslakov, S. V. Savilov and V. Lunin, *Appl. Surf. Sci.*, 2020, **507**, 145027.
11 F. Arcudi, L. Đorđević, S. Rebeccani, M. Cacioppo, A. Zanut, G. Valenti, F. Paolucci and M. Prato, *Adv. Sci.*, 2021, **8**, 2100125.
12 C. Wang, X. Wu, X. Li, W. Wang, L. Wang, M. Gu and Q. Li, *J. Mater. Chem.*, 2012, **22**, 15522.
13 M. Luo, Y. Hua, Y. Liang, J. Han, D. Liu, W. Zhao and P. Wang, *Biosens. Bioelectron.*, 2017, **98**, 195–201.
14 C. Rosso, G. Filippini and M. Prato, *ACS Catal.*, 2020, **10**, 8090–8105.
15 W. Zhou, J. Zhuang, W. Li, C. Hu, B. Lei and Y. Liu, *J. Mater. Chem. C*, 2017, **5**, 8014–8021.
16 S. Yang, J. Sun, X. Li, W. Zhou, Z. Wang, P. He, G. Ding, X. Xie, Z. Kang and M. Jiang, *J. Mater. Chem. A*, 2014, **2**, 8660.
17 D. Saini, A. Garg, C. Dalal, S. R. Anand, S. K. Sonkar, A. K. Sonker and G. Westman, *ACS Appl. Nano Mater.*, 2022, **5**, 3087–3109.
18 X. Kou, S. Jiang, S.-J. Park and L.-Y. Meng, *Dalton Trans.*, 2020, **49**, 6915–6938.
19 S. Hu, Q. Chang, K. Lin and J. Yang, *Carbon*, 2016, **105**, 484–489.
20 X. Qu, C. Gao, L. Fu, Y. Chu, J. Wang, H. Qiu and J. Chen, *ACS Appl. Mater. Interfaces*, 2023, **15**, 18608–18619.
21 W. Yang, J. Ni, F. Luo, W. Weng, Q. Wei, Z. Lin and G. Chen, *Anal. Chem.*, 2017, **89**, 8384–8390.
22 A. Dutta and S. K. Gogoi, *Anal. Methods*, 2024, **16**, 8204–8215.
23 L. Li, C. Lu, S. Li, S. Liu, L. Wang, W. Cai, W. Xu, X. Yang, Y. Liu and R. Zhang, *J. Mater. Chem. B*, 2017, **5**, 1935–1942.
24 H. Li, X. Yan, D. Kong, R. Jin, C. Sun, D. Du, Y. Lin and G. Lu, *Nanoscale Horiz.*, 2020, **5**, 218–234.
25 T. Feng, S. Tao, D. Yue, Q. Zeng, W. Chen and B. Yang, *Small*, 2020, **16**, 2001295.
26 X. Li, M. Rui, J. Song, Z. Shen and H. Zeng, *Adv. Funct. Mater.*, 2015, **25**, 4929–4947.
27 M. Han, S. Zhu, S. Lu, Y. Song, T. Feng, S. Tao, J. Liu and B. Yang, *Nano Today*, 2018, **19**, 201–218.
28 H. Kaurav, D. Verma, A. Bansal, D. Kapoor and S. Sheth, *Front. Chem.*, 2023, **11**, 1–22.
29 Q. Wang, X. Huang, Y. Long, X. Wang, H. Zhang, R. Zhu, L. Liang, P. Teng and H. Zheng, *Carbon*, 2013, **59**, 192–199.
30 V. M. Naik, D. B. Gunjal, A. H. Gore, S. P. Pawar, S. T. Mahanwar, P. V. Anbhule and G. B. Kolekar, *Diam. Relat. Mater.*, 2018, **88**, 262–268.
31 S. Bhandari, D. Mondal, S. K. Nataraj and R. G. Balakrishna, *Nanoscale Adv.*, 2019, **1**, 913–936.

32 Y. Choi, X. T. Zheng and Y. N. Tan, *Mol. Syst. Des. Eng.*, 2019, **5**, 67–90.
33 P. Dubey, *RSC Adv.*, 2023, **13**, 35088–35126.
34 H. Liu, X. Zhong, Q. Pan, Y. Zhang, W. Deng, G. Zou, H. Hou and X. Ji, *Coord. Chem. Rev.*, 2024, **498**, 215468.
35 S. Chahal, J.-R. Macairan, N. Yousefi, N. Tufenkji and R. Naccache, *RSC Adv.*, 2021, **11**, 25354–25363.
36 V. Bressi, A. M. Balu, D. Iannazzo and C. Espro, *Curr. Opin. Green Sustain. Chem.*, 2023, **40**, 100742.
37 M. Alafeef, I. Srivastava, T. Aditya and D. Pan, *Small*, 2023, **20**, 2303937.
38 H. Laddha, P. Yadav, P. Sharma, M. Agarwal and R. Gupta, *J. Ind. Eng. Chem.*, 2023, **131**, 257–264.
39 H. Liu and S. Wu, *J. Mol. Struct.*, 2025, **1329**, 141459.
40 L. Ma, C. Ma, G. Chen, J. Gu, T. Yang, L. Li, H. Gao, Y. Xiong, Y. Wu, C. Zhu, Y. Zhou, A. Hu, K. Chen and Z. Liu, *J. Fluoresc.*, 2024, **35**, 1807–1817.
41 Y. Wang, R. Wu, Y. Zhang, S. Cheng, B. Wang, Y. Zhang and Y. Zhang, *Spectrochim. Acta, Part A*, 2024, **308**, 123709.
42 E. K. Adotey, M. AmoueiTorkmahalleh, L. Tastanova, A. Bekeshev, D. Shah, P. K. Hopke, W. Lee and M. P. Balanay, *J. Hazard. Mater.*, 2024, **462**, 132671.
43 Z. Yang, T. Xu, S. Zhang, H. Li, Y. Ji, X. Jia and J. Li, *Nano Res.*, 2022, **16**, 5401–5411.
44 N. Tuccitto, L. Fichera, R. Ruffino, V. Cantaro, G. Sfuncia, G. Nicotra, G. T. Sfrazzetto, G. Li-Destri, A. Valenti, A. Licciardello and A. Torrisi, *ACS Appl. Nano Mater.*, 2021, **4**, 6250–6256.
45 C. Gar, M. Rottenkolber, C. Prehn, J. Adamski, J. Seissler and A. Lechner, *Crit. Rev. Clin. Lab. Sci.*, 2017, **55**, 21–32.
46 N. Killiny, Y. Nehela, F. Hijaz and C. I. Vincent, *Virulence*, 2017, **9**, 99–109.
47 F. Zhang, X. Ma, H. Li, G. Guo, P. Li, H. Li, L. Gu, X. Li, L. Chen and X. Zhang, *Urol. Oncol.*, 2017, **35**, 392–400.
48 D. Yang, L. Lu, S. Feng and M. Zhu, *Dalton Trans.*, 2020, **49**, 7514–7524.
49 A. D'Aniello, J. M. Lee, L. Petrucelli and M. M. Di Fiore, *Neurosci. Lett.*, 1998, **250**, 131–134.
50 Y. Zhou and J. Yoon, *Chem. Soc. Rev.*, 2012, **41**, 52–67.
51 H. J. Issaq and K. C. Chan, *Electrophoresis*, 1995, **16**, 467–480.
52 H. Imanzadeh, Y. Sefid-Sefidehkhan, H. Afshary, A. Afruz and M. Amiri, *J. Pharm. Biomed. Anal.*, 2023, **230**, 115390.
53 P. Chauhan, D. Mundekkad, A. Mukherjee, S. Chaudhary, A. Umar and S. Baskoutas, *Nanomaterials*, 2022, **12**, 162.
54 Y. Z. Yang, N. Xiao, S. G. Liu, L. Han, N. B. Li and H. Q. Luo, *Mater. Sci. Eng., C*, 2020, **108**, 110401.
55 P. Chauhan, J. Saini, S. Chaudhary and K. K. Bhasin, *Mater. Res. Bull.*, 2021, **134**, 111113.
56 R. Tabaraki and O. Abdi, *J. Fluoresc.*, 2019, **29**, 751–756.
57 J. Peng, W. Gao, B. K. Gupta, Z. Liu, R. Romero-Aburto, L. Ge, L. Song, L. B. Alemany, X. Zhan, G. Gao, S. A. Vithayathil, B. A. Kaipparettu, A. A. Marti, T. Hayashi, J.-J. Zhu and P. M. Ajayan, *Nano Lett.*, 2012, **12**, 844–849.
58 Z. Wang, B. Huang, Y. Dai, Y. Liu, X. Zhang, X. Qin, J. Wang, Z. Zheng and H. Cheng, *CrystEngComm*, 2012, **14**, 1687–1692.
59 X. Hong, W. Yu, A. Wang and D. D. L. Chung, *Carbon*, 2016, **109**, 874–882.
60 J. Barkauskas, J. Gaidukevič and G. Niaura, *Carbon Lett.*, 2021, **31**, 1097–1110.
61 Y. Zhang, Y. H. He, P. P. Cui, X. T. Feng, L. Chen, Y. Z. Yang and X. G. Liu, *RSC Adv.*, 2015, **5**, 40393–40401.
62 S.-W. Hao, C.-H. Hsu, Y.-G. Liu and B. K. Chang, *RSC Adv.*, 2016, **6**, 109950–109959.
63 M. Chatterjee, P. Nath, S. Kadian, A. Kumar, V. Kumar, P. Roy, G. Manik and S. Satapathi, *Sci. Rep.*, 2022, **12**, 9061.
64 V. S. Smitha, P. Athulya, K. K. Jayasooryan and T. R. Resmi, *Environ. Sci.:Adv.*, 2024, **3**, 1400–1412.
65 D. Bano, V. Kumar, S. Chandra, V. K. Singh, S. Mohan, D. K. Singh, M. Talat and S. H. Hasan, *Opt. Mater.*, 2019, **92**, 311–318.
66 S. Liao, X. Zhao, F. Zhu, M. Chen, Z. Wu, X. song, H. Yang and X. Chen, *Talanta*, 2018, **180**, 300–308.
67 D. K. Dang, S. Chandrasekaran, Y.-L. T. Ngo, J. W. Chung, E. H. Kim and S. H. Hur, *Sens. Actuators, B*, 2018, **255**, 3284–3291.
68 J. Chen, J.-S. Wei, P. Zhang, X.-Q. Niu, W. Zhao, Z.-Y. Zhu, H. Ding and H.-M. Xiong, *ACS Appl. Mater. Interfaces*, 2017, **9**, 18429–18433.
69 K. Holá, M. Sudolská, S. Kalytchuk, D. Nachtigallová, A. L. Rogach, M. Otyepka and R. Zbořil, *ACS Nano*, 2017, **11**, 12402–12410.
70 S. Sun, L. Zhang, K. Jiang, A. Wu and H. Lin, *Chem. Mater.*, 2016, **28**, 8659–8668.
71 Y. Wang, S. W. Kim and L. Feng, *Anal. Chim. Acta*, 2015, **890**, 134–142.
72 J. Shen, T. Zhang, Y. Cai, X. Chen, S. Shang and J. Li, *New J. Chem.*, 2017, **41**, 11125–11137.
73 Q. Liu, X. Niu, Y. Zhang, Y. Zhao, K. Xie, B. Yang, Q. He, S. Lv and L. Li, *Nanoscale*, 2020, **12**, 13010–13016.
74 C. Wang, C. Pan, X. Wei, F. Yang, W. Wu and L. Mao, *Talanta*, 2020, **208**, 120375.
75 D. Qu, M. Zheng, P. Du, Y. Zhou, L. Zhang, D. Li, H. Tan, Z. Zhao, Z. Xie and Z. Sun, *Nanoscale*, 2013, **5**, 12272.
76 D. Wang, X. Wang, Y. Guo, W. Liu and W. Qin, *RSC Adv.*, 2014, **4**, 51658–51665.
77 X. Hao, L. Huang, C. Zhao, S. Chen, W. Lin, Y. Lin, L. Zhang, A. Sun, C. Miao, X. Lin, M. Chen and S. Weng, *Mater. Sci. Eng., C*, 2021, **123**, 111971.
78 E. H. H. Hasabeldaim, H. C. Swart and R. E. Kroon, *RSC Adv.*, 2023, **13**, 5353–5366.
79 Y. Su, E. P. Hessou, E. Colombo, G. Belletti, A. Moussadik, I. T. Lucas, V. Frochot, M. Daudon, S. Rouzière, D. Bazin, K. Li, P. Quaino and F. Tielens, *Amino Acids*, 2022, **54**, 1123–1133.
80 D. Genovese, M. Cingolani, E. Rampazzo, L. Prodi and N. Zaccheroni, *Chem. Soc. Rev.*, 2021, **50**, 8414–8427.
81 B. Valeur and M. N. Berberan-Santos, in *Molecular Fluorescence Principles and Applications*, Willey-VCH, Germany, 2nd edn., 2012.
82 J. R. Lakowicz, in *Principles of Fluorescence Spectroscopy*, Springer US, Boston, MA, 2006.
83 J. Hu, Y. Sun, A. A. Aryee, L. Qu, K. Zhang and Z. Li, *Anal. Chim. Acta*, 2022, **1209**, 338885.